Photochemical & Photobiological Sciences

PAPER

Cite this: *Photochem. Photobiol. Sci.*, 2018, **17**, 414

A novel Schiff base derivative of pyridoxal for the optical sensing of Zn^{2+} and cysteine†

Thangaraj Anand, [a] Ashok S. K. Kumar [b] and Suban K. Sahoo *[a]

Received 20th October 2017,
Accepted 12th February 2018

DOI: 10.1039/c7pp00391a

rsc.li/pps

An easy to prepare novel vitamin B_6 cofactor derivative 3-hydroxy-*N*′-((3 hydroxy-5-(hydroxymethyl)-2-methylpyridin-4-yl)methylene)-2-naphthohydrazide (**NPY**) was synthesized by a one pot condensation reaction of pyridoxal with 3-hydroxy-2-naphthoic hydrazide and applied for the optical detection of Zn^{2+} and cysteine in the aqueous DMSO medium. The addition of Zn^{2+} ions leads to a selective blue-shift in the fluorescence emission spectrum of **NPY** from 530 nm to 475 nm, which allowed ratiometric detection of Zn^{2+} ions down to 8.73×10^{-7} M without any interference from other tested metal ions. This system was also successfully applied to detect intracellular Zn^{2+} ions in live HeLa cells. Further, when the *in situ* generated **NPY**·Zn^{2+} complex was interacted with various amino acids, the addition of cysteine resulted in an instantaneous colour change from light yellow to colourless and the absorbance at 435 nm of the complex was quenched selectively. Also, the fluorescence of the **NPY**·Zn^{2+} complex was quenched, which allowed the detection of cysteine down to 6.63×10^{-7} M.

1. Introduction

The development of new fluorescent chemosensors and transporters for detecting ionic species and amino acids is continuing to see an upsurge of interest in supramolecular chemistry.[1] Next to iron, zinc is the second most abundant transition metal ion in the human body and it appears in the enzymes dispersed all over the human body.[2] Zn^{2+} derived compounds are extensively used in medical fields as tumor photosensitizers, antibacterial/antimicrobial and anticancer agents, radioprotective agents and antidiabetic insulin mimetics.[3] In blood serum, the total concentration of zinc is 10 μM.[4] Yet, the exact biological roles of zinc are still not entirely known. On the other side, zinc dysbolism is the main cause for human diseases.[5] The scarcity of zinc in the human body causes intellectual disability, digestive dysfunction, loss of brain function, gene transcription, immune deficiency, mammalian reproduction disorder,[6] *etc.*, Also, the metal ions like Cu^{2+}, Zn^{2+}, and Fe^{2+} play key roles in the aggregation of β-amyloid peptides during the onset of Alzheimer's disease[7] and other neurological diseases like Parkinson's disease, cerebral ischemia and epilepsy.[8] Zinc pollution occurs from electroplating industries and its toxicity has been found in both acute and chronic forms. In addition, the soil microbial activity may be reduced by Zn^{2+}, a common contaminant in agricultural and food wastes.[9] Therefore, the detection of Zn^{2+} in biological and environmental systems is of great importance.

Amino acids are building blocks for proteins. Cysteine (Cys), homocysteine (Hcy), and glutathione (GSH) are the important mercapto amino acids required for cell growth and tissues in living organisms.[10] Cysteine is very important among the 20 essential amino acids because of its free thiol moiety. Abnormal levels of thiols can reflect diseases like liver damage, cancer, osteoporosis, AIDS, *etc.*[11] Cys is used in neurotoxins, biomarkers and physiological regulators.[12] Precisely, the lack of Cys causes many syndromes, for instance, slow growth in children, hair depigmentation, edema, lethargy, neurotoxicity, liver damage, loss of muscle and fat, skin lesions, and weakness.[13] Thus, it is important to develop efficient, sensitive methods for the detection and quantification of biothiols in physiological media for academic research and clinical applications.

At present, a range of detection methods for Zn^{2+} ions have been developed, such as electrochemical, inductively coupled plasma mass spectrometry, and atomic absorption spectroscopy methods.[14] These analytical methods have both advantages and disadvantages, whereas, the optical detection methods such as colorimetry and fluorimetry[15] opted in chemosensor chemistry are most advantageous due to their simplicity, high sensitivity, ready availability, low cost and their applicability in living cells (*in vivo*) for the detection of guest in designing such chemosensors possessing both a light-emitting unit and a guest binding site. The Schiff base

[a]*Department of Applied Chemistry, S. V. National Institute of Technology (SVNIT), Surat-395007, India. E-mail: suban_sahoo@rediffmail.com; Tel: +91-261-2201814*
[b]*Materials Chemistry Division, School of Advanced Sciences, VIT University, Vellore-632014, India. E-mail: sks@chem.svnit.ac.in*

†Electronic supplementary information (ESI) available. See DOI: 10.1039/c7pp00391a

ligands are very useful in the designing of chemosensors because of their high yield synthesis by a simple one pot condensation reaction[16] and also the fascinating coordinative behavior toward the transition metal ions. Considering the above facts, we have synthesized a new Schiff base receptor **NPY** by reacting 3-hydoxy-2-naphthoic hydrazide with pyridoxal under reflux conditions (Scheme 1). The biological importance of the non-phosphate form of vitamin B_6 cofactor *i.e.*, pyridoxal and its derivatives, is well established along with their fascinating coordination and optical properties,[17] but very few reports on the development of chemosensors utilizing the pyridoxal platform are present.[18] The receptor **NPY** recognizes Zn^{2+} with a significant blue-shift in the fluorescence spectrum due to the formation of the **NPY**·Zn^{2+} complex. The resulting **NPY**·Zn^{2+} complex detects cysteine by dual modes: the absorbance and fluorescence of the **NPY**·Zn^{2+} complex were quenched selectively among the other tested amino acids.

2. Experimental

2.1 Materials and instrumentations

Pyridoxal hydrochloride and 3-hydroxy-2-naphthoic hydrazide were purchased from Sigma–Aldrich. All the solvents were of analytical grade and used without further purification. Metal salts of Cu^{2+}, Co^{2+}, Ni^{2+}, Mn^{2+}, Mg^{2+}, Fe^{3+}, Fe^{2+}, Zn^{2+}, Cd^{2+}, Hg^{2+}, Pb^{2+}, Al^{3+}, and Cr^{3+} ions and the amino acids such as aspartic acid (Asp), cysteine (Cys), alanine (Ala), arginine (Arg), glycine (Gly), histidine (His), leucine (Leu), methionine (Met), proline (Pro), serine (Ser), threonine (Thr), tryptophan (Trp), lysine (Lys) and glutamic acid (Glu) were obtained from Merck.

The ^{1}H and ^{13}C NMR spectra were recorded on a Bruker (Advance) 300 MHz instrument. The UV-Vis absorption spectra were recorded on a Cary 50 Varian UV-Vis spectrophotometer at room temperature using quartz cells of 1.0 cm optical path length in the range of 300–700 nm. The fluorescence spectra were obtained on a Cary Eclipse Fluorescent spectrophotometer in the emission range of 380–800 nm by keeping the slit width 5 : 5 nm and excitation wavelength 375 nm. The FT-IR spectrum from 4000 to 600 cm^{-1} was recorded by using a Shimadzu IR Affinity FTIR. The high resolution mass spectra were recorded by using a Xevo G2-S Q TOF instrument in positive mode. Fluorescein (Φ = 0.79) in 0.1 M NaOH was used as a standard for the quantum yield calculations.

For the various sensing experiments, the stock solution of the receptor **NPY** (1 mM) was prepared in DMSO, whereas the cations and amino acid (1 mM) solutions were prepared using double distilled water. These solutions were used for all the spectroscopy studies after appropriate dilution. The fluorescence selectivity experiment was performed by taking 100 μL of **NPY** (1 mM, DMSO) in a series of vials and then was diluted with 1850 μL DMSO followed by the addition of 50 μL of the different metal ions (1 mM, H_2O). Then, the fluorescence spectra were recorded at λ_{exc} = 375 nm. The same vials were also used to record the UV-Vis spectra. This solvent condition was used because of the insolubility of **NPY** in aqueous medium and to obtain the proper selectivity for the target analyte.

2.2 Synthesis of NPY

Ethanolic solution containing 3-hydoxy-2-naphthoic hydrazide (0.154 g, 0.74 mmol) and pyridoxal hydrochloride (0.080 g, 0.74 mmol) with the adjustment of pH to 7 by using NaOH was refluxed for two hours. The excess solvent was distilled off under reduced pressure. The lime yellow powder was obtained and washed with diethyl ether. Recrystallization with hot ethanol gives a lime yellow powder product. Yield: 73%. ATR-FTIR (cm^{-1}): 3218, 3053, 1691, 1665, 1551. ^{1}H NMR (300 MHz, δ, ppm, DMSO-d_6): 12.69 (s, 2H), 11.30 (s, 1H), 9.02 (s, 1H), 8.50 (s, 1H), 8.06 (s, 1H), 7.94 (d, J = 8.3 Hz, 1H), 7.78 (d, J = 8.3 Hz, 1H), 7.66–7.45 (m, 1H), 7.53–7.11 (m, 2H), 5.58 (s, 1H), 4.69 (s, 2H), 2.50 (s, 3H). ^{13}C NMR (75 MHz, δ, ppm, DMSO-d_6): 164.59, 154.61, 152.12, 147.03, 146.92, 146.83, 143.71, 136.90, 131.82, 129.50, 129.36, 127.61, 126.70, 124.75, 122.97, 120.52, 111.46, 58.83, 17.99; HRMS: calculated: 351.122 $(M + H)^+$, found: 352.007.

2.3 *In vitro* cellular imaging

Localization of **NPY** and the ability of **NPY** for Zn^{2+} recognition were investigated in live HeLa cell lines. Briefly, HeLa cells (7 × 103 cells per well) were seeded on to 96 well cell carrier microplates (PerkinElmer, US). When the cells reached 80% confluence, the media were changed. Cells were then treated with 10 μM of **NPY** alone and supplemented with Zn^{2+} (10 μM) and the plate was incubated for 30 minutes in a humidified incubator at 37 °C with 5% CO_2. The cells were washed twice with PBS buffer, and then the fluorescence images of the cells were recorded by using an Olympus SV 1000 confocal fluorescence Microscopy.

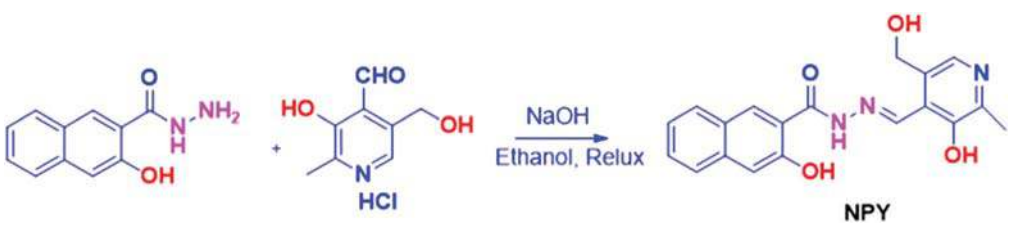

Scheme 1 Synthetic route of the receptor **NPY**.

3. Results and discussion

3.1. Synthesis and characterization

The receptor **NPY** was prepared by a one pot condensation reaction of 3-hydroxy-2-naphthoic hydrazide with pyridoxal in ethanol under refluxing conditions, which furnished the product **NPY** in an excellent yield of 73% (Scheme 1). The structure of **NPY** was confirmed by ^{1}H NMR, ^{13}C-NMR, FT-IR and HRMS spectroscopy (Fig. S1–S4†). The ATR-FTIR spectral analysis indicates that the ν_{NH2} and ν_{OH} peaks of **NPY** were observed respectively at 3053 cm^{-1} and 3218 cm^{-1} whereas the $\nu_{C=O}$ band appeared at 1691 cm^{-1}. The imine $\nu_{C=N}$ stretching band was observed at 1665 cm^{-1}. In ^{1}H NMR, the naphthyl-OH and amide-NH give a singlet peak at 12.69 ppm, and a pyridoxal-OH peak at 11.30 ppm, whereas the characteristic imine proton peak was observed at 9.02 ppm. A sharp singlet at 8.50 ppm was characterized for the pyridoxal aromatic proton whereas other naphthyl aromatic peaks were observed between 6 ppm and 8 ppm. The alcoholic-OH gives a sharp peak at 5.58 ppm, whereas the peak for the methyl group was observed at 2.50 ppm. In ^{13}C NMR, the carbonyl carbon was observed around 164.59 ppm. The imine carbon was observed at 146.92 ppm and all the aromatic carbons peaks were observed in the range of 110–140 ppm. Methyl and methylene carbons were observed at 58.83 ppm and 17.99 ppm, respectively. Finally, the structure of **NPY** was confirmed by using the mass data and then applied for the detection of cations.

3.2. Fluorescence studies of NPY with metal ions

The probe **NPY** (2 mL, 5 × 10^{-5} M, DMSO) displays a broad emission band (Φ = 0.13 compared to fluorescein Φ = 0.79) with maxima at ~530 nm on excitation at 375 nm due to the extended π-electronic structure and push–pull effect of naphthyl and pyridoxal units, and shows the light yellow fluorescent colour under UV-light (365 nm). The fluorescence response of **NPY** was investigated with various cations (50 μL, 1 × 10^{-3} M, H_2O) such as Cu^{2+}, Co^{2+}, Ni^{2+}, Mn^{2+}, Mg^{2+}, Fe^{2+}, Fe^{3+}, Zn^{2+}, Cd^{2+}, Hg^{2+}, Pb^{2+}, Al^{3+} and Cr^{3+} (Fig. 1a and Fig. S5†). When Zn^{2+} was added to the solution of **NPY**, the probe emission intensity decreased and selectively blue-shifted to 475 nm (Φ = 0.02). However, the addition of other metal ions induced either negligible change or quenching in the fluorescence profile of **NPY**, but the blue-shifted emission band was observed only in the presence of Zn^{2+} that allowed selective ratiometric detection. The bar representation of the emission ratio I_{475}/I_{530} of **NPY** in the presence of different metal ions clearly supported the high selective nature of **NPY** as a ratiometric fluorescent sensor for Zn^{2+} ions (Fig. 1a).

To elicit the interaction between **NPY** and Zn^{2+} ions, the fluorescence titration of **NPY** (2 mL, 5 × 10^{-5} M, DMSO) was performed by the incremental addition of Zn^{2+} (5 μL, 1 × 10^{-4} M, H_2O) ions (Fig. 1b). Upon the successive addition of an incremental amount of Zn^{2+} to the probe **NPY** solution, the emission band at ~530 nm started decreasing and instantaneously a new blue shifted band was observed at 475 nm with the formation of an isosemissive point at 492 nm. This result supported the formation of a new complex species in solution due to the complexation reaction that occurred between the probe **NPY** and Zn^{2+} presumably *via* the pyridoxal-OH, carbonyl-O and imine-N. Upon complexation, the ICT of receptor **NPY** was affected due to the chelation of receptor **NPY** with Zn^{2+}, which ultimately resulted in blue shifting of the emission spectrum of the receptor.[19]

To further investigate the tolerance of **NPY** (2 mL, 5 × 10^{-5} M, DMSO) with Zn^{2+} (50 μL, 1 × 10^{-3} M, H_2O) with other competitive metal ions (50 μL, 1 × 10^{-3} M, H_2O) such as Cu^{2+}, Co^{2+}, Ni^{2+}, Mn^{2+}, Mg^{2+}, Fe^{2+}, Fe^{3+}, Cd^{2+}, Hg^{2+}, Pb^{2+}, Al^{3+} and Cr^{3+}, the cross sensitivity experiments were conducted (Fig. 2a). The competition experiments revealed that the Zn^{2+} induced fluorescence enhancement at 475 nm was unaffected, even in the presence of other tested interfering metal ions. This result confirms that **NPY** is highly specific and can be applied for the fluorescent ratiometric detection of Zn^{2+} ions. From the fluorescence titration data, the limit of detection (LOD) of the

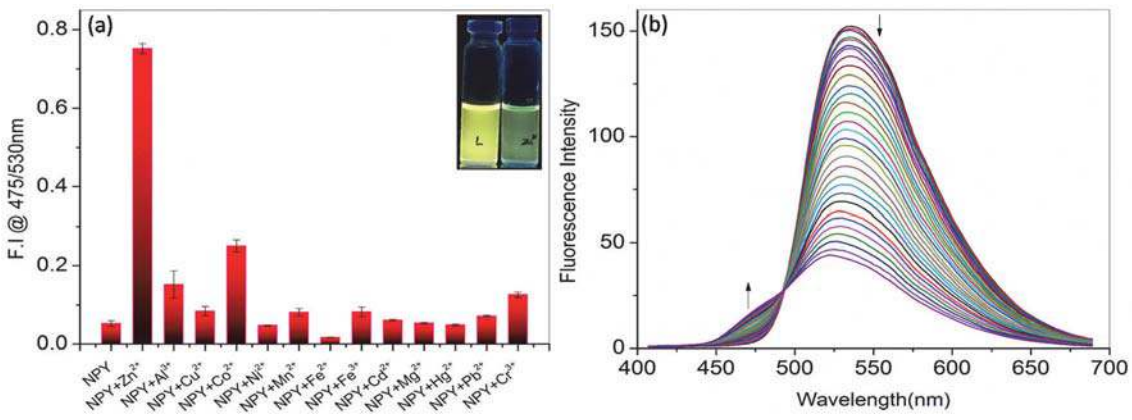

Fig. 1 (a) Selective emission spectra (I_{475}/I_{530}) of **NPY** (2 mL, 5 × 10^{-5} M, DMSO) upon the addition of Zn^{2+} ions (50 μL, 1 × 10^{-3} M, H_2O) and other metal ions (inset shows the fluorescent vials observed under UV light). (b) Fluorescence titration of **NPY** (2 mL, 5 × 10^{-5} M, H_2O) with a successive incremental addition of Zn^{2+} (5 μL, 1 × 10^{-4} M, H_2O).

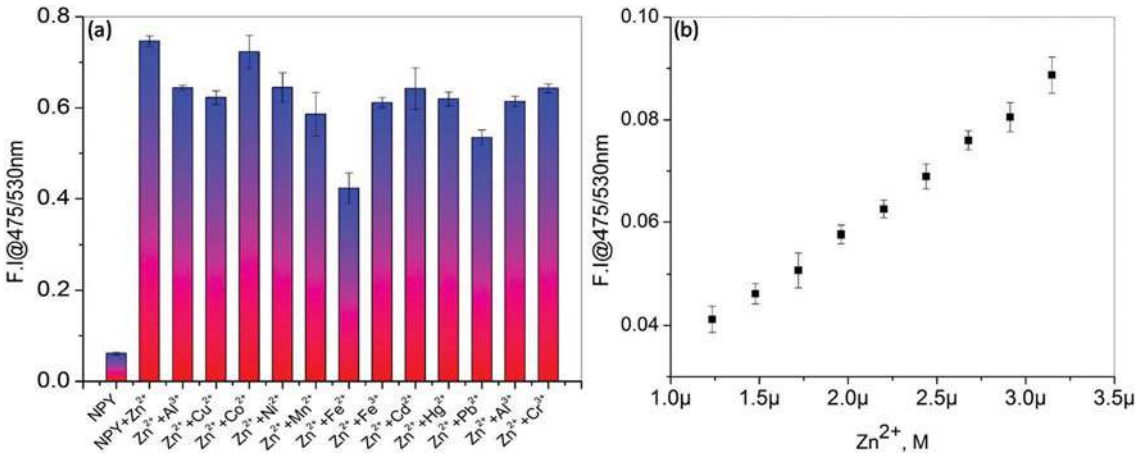

Fig. 2 (a) Fluorescence intensity ratio I_{475}/I_{530} of the receptor **NPY** (2 mL, 5×10^{-5} M, DMSO) after adding Zn^{2+} (50 μL, 1×10^{-3} M, H_2O) ions and equimolar concentration of other competitive cations (50 μL, 1×10^{-3} M, H_2O). (b) Calibration curve for calculating the limit of detection of **NPY** with Zn^{2+}.

probe **NPY** for Zn^{2+} was estimated down to 8.73×10^{-7} M by applying the standard IUPAC method of 3σ/slope (where σ represents the standard deviation of the blank sample (Fig. 2b)). The estimated detection limit for Zn^{2+} was far better than the acceptable limit of 76×10^{-6} M of Zn^{2+} suggested by the US-EPA and World Health Organization (WHO) for drinking water.[20] Also, the novelty of **NPY** was checked by comparing with the analytical results of some reported naphthyl based sensors (Table S1†) and other reported official methods (Table S2†), which revealed that the probe **NPY** showed comparable/superior analytical performance.

The binding constant K_a was evaluated from the fluorescence titration profile by using the Benesi–Hildebrand equation[21] *i.e.*, $1/(F_\infty - F_0) = 1/(F_\infty - F_0)\ K\ [G] + 1/(F - F_0)$. Where, F_0 represents the fluorescence intensity in the absence of the analyte, F represents the fluorescence intensity in the presence of the analyte, F_∞ represents the fluorescence intensity after titration and [G] represents the concentration of the analyte. The binding constant of 6.1×10^5 M^{-1} was estimated from the Benesi–Hildebrand plot for the complex species formed between **NPY** and Zn^{2+} (Fig. S6†). The Benesi–Hildebrand plot fitted well for the 1 : 1 binding stoichiometry between **NPY** and Zn^{2+}. To further confirm that the complex formation occurred between the **NPY** and Zn^{2+} ion, the zinc complex was isolated in the solid state and characterized. The solid complex was obtained as orange-yellow colored flakes and showed the absorbance maxima at λ_{abs} = 317 nm, 332 nm, 408 nm and 435 nm (Fig. S7a†) whereas the emission maxima were (λ_{exc} = 375 nm) at λ_{em} = 475 nm and 525 nm (Fig. S7b†). The observed spectral data of the isolated **NPY**·Zn^{2+} complex showed good agreement with the complex species formed in the solution state (Fig. S7†). Furthermore, the 1 : 1 complex formation between **NPY** and Zn^{2+} was confirmed by the HRMS data which revealed the molecular ion peak at m/z = 450.29 assigned for the species (Zn(**NPY**-H^+)Cl^-, Fig. S8†). Furthermore, the effect of pH for the detection of Zn^{2+} ions by **NPY** was tested by recording the fluorescence spectra at different pH values from 2 to 12 (Fig. S9†). The results revealed that the receptor **NPY** can be applied to detect Zn^{2+} above pH = ~6.5. At lower pH, the protonated form of **NPY** restricts the complexation with Zn^{2+} and therefore no significant fluorescence changes of **NPY** were observed in the absence and presence of Zn^{2+}.

3.3. Intracellular live cell imaging

Considering the biological importance of Zn^{2+} and its detection in intracellular components, the potential utility of **NPY** for monitoring Zn^{2+} in living cells was examined. The fluorescence imaging studies in live HeLa cells with the probe **NPY** were performed in the presence and absence of Zn^{2+} ions by using the confocal fluorescence microscopy (Fig. 3). In the present study, the HeLa cells were first incubated with probe **NPY** (10 μM) for 30 minutes at 37 °C and washed with PBS solution, and then the cells were exposed to fluorescence imaging which shows cell permeability and fluorescence. Further Zn^{2+} (10 μM) ions were added into the probe **NPY** treated cells for 10 min at 37 °C, and images were taken. The images summarized in Fig. 3 indicate that the yellow fluorescent cells in the presence of **NPY** were changed to blue fluorescent cells in the presence of Zn^{2+} due to the complex formation that occurred between Zn^{2+} and the probe **NPY** within the HeLa cells. These results confirm that the probe **NPY** is cell permeable and can be applied as a sensor to detect Zn^{2+} in living cells.

3.4. Complexation studies of NPY with metal ions

The Zn^{2+} ion recognition ability of **NPY** (5×10^{-5} M, DMSO) was investigated by recording the UV-Vis absorbance spectra. The probe shows a broad absorption between 300 nm and 450 due to the mixed π to π* and n–π* transitions. After the addition of Zn^{2+} (50 μL, 1×10^{-3} M, H_2O), an obvious decrease in the absorbance at 385 nm occurred and concomitantly the

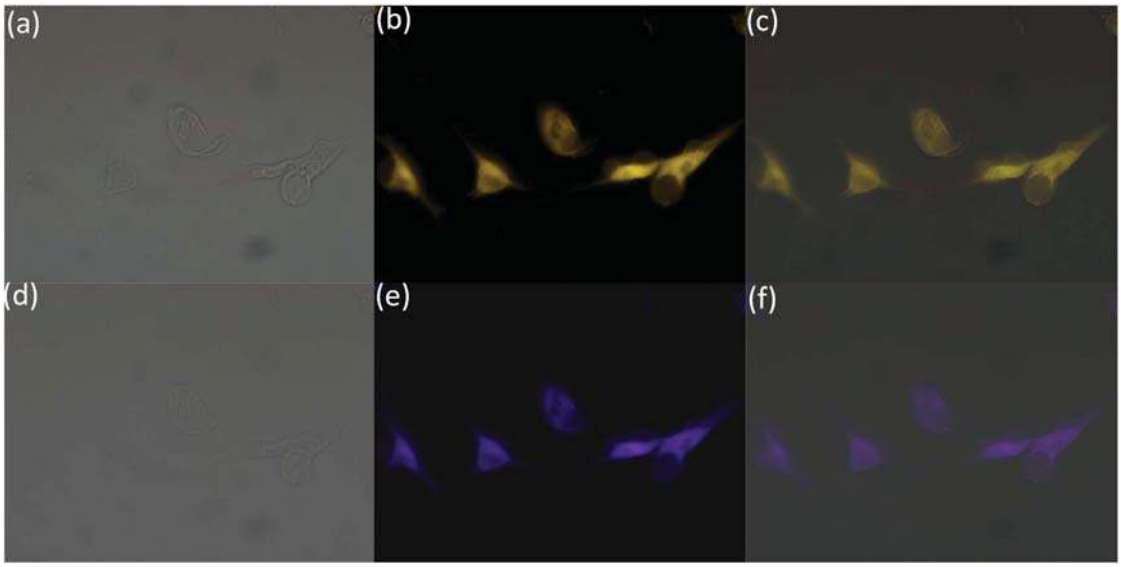

Fig. 3 (a) Bright field image of HeLa cells with **NPY** (10 μM), (b) confocal fluorescence image of cells incubated with **NPY** alone without Zn^{2+}, (c) merged image of **NPY**, (d) Bright field image HeLa cells with **NPY** (10 μM) and Zn^{2+} (10 μM), (e) confocal fluorescence image of cells with **NPY** and Zn^{2+} and (f) merged image of **NPY** with Zn^{2+}.

intensity of the peak at 435 nm increased (Fig. S7†). The spectral changes associated with the naked eye detectable colour change from colourless to yellow (Fig. S10†) supported the formation of the **NPY**·Zn^{2+} complex in the ground state. Further, to get fuller insight into the possible binding modes of **NPY** with Zn^{2+} ions, ^{1}H-NMR titration was performed in DMSO-d_6 (Fig. 4). The ^{1}H NMR spectrum of **NPY** displayed characteristic amide NH and hydroxyl OH protons at 12.69 ppm, and the other aliphatic and aromatic protons in their respective positions. In the ^{1}H NMR titration experiments, the increasing

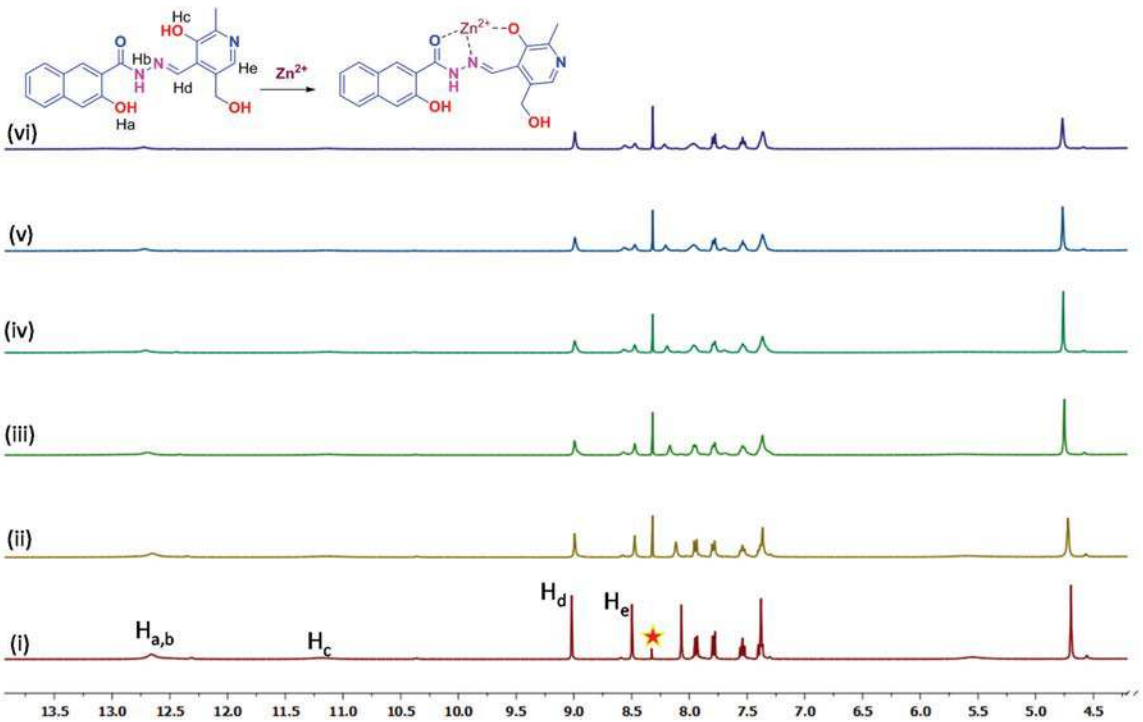

Fig. 4 ^{1}H-NMR spectrum of **NPY** with an incremental addition of Zn^{2+} ions in DMSO-d_6 [equivalents of Zn^{2+} with respect to **NPY**: 0 (i), 0.2 (ii), 0.4 (iii), 0.6 (iv), 0.8 (v) and 1.0 (vi)]. *The peak appeared because some pyridoxal-N may be under protonated conditions.

addition of zinc to a solution of **NPY** results in the disappearance of phenolic hydroxyl protons at 11.30 ppm. At the same time, imine protons at 9.02 ppm show a negligible shift in the presence of zinc ions. These results suggest that the imine and hydroxyl group interactions are a crucial driving force for the complex formations along with the carbonyl-O which can be ascertained from the downfield shift of the peak at 12.69 ppm.

Based on the experimental evidence, the possible 3D structure of **NPY** and its complex with Zn^{2+} was proposed theoretically by applying the density functional theory (DFT) method. The DFT optimization of the structure was performed by using the B3LYP exchange–correlation functional and the basis sets 6–31G** for the N, O, C, and H atoms whereas LANL2DZ for the Zn atom. All calculations were performed by using the computational code Gaussian 09 W.[22] As shown in Fig. 5a, the receptor **NPY** preferred a planar structure with a strong intramolecular hydrogen bonding between the pyridoxal-OH and imine-N of length 1.755 Å. Based on the obtained optimized structure of **NPY**, no apparent conformation changes are required to coordinate the Zn^{2+} ion (Fig. 5b). Also, the calculated interaction energy ($E_{int} = E_{complex} - E_{receptor} - 2E_{Zn^{2+}}$) for the complexation between **NPY** and Zn^{2+} was lowered by −109.55 kcal mol^{-1}, which supported the formation of a stable complex. Further analysis of the band gap ($\Delta E = E_{LUMO} - E_{HOMO}$) between the highest occupied molecular orbital (HOMO) and lowest unoccupied molecular orbital (LUMO) of **NPY** (0.1386 eV) on complexation with Zn^{2+} (0.1115 eV) complemented well the red-shift in the absorption band upon complexation (Fig. S7†).

3.5 Fluorescence studies of zinc complex with amino acids

The biomolecules such as amino acids can snatch the coordinated metal ions from the receptor conducing the recovery of the fluorescence of the receptor which allowed us to develop a sequential sensor with the same receptor. With this approach, the **NPY**·Zn^{2+} complex solution was prepared by mixing **NPY** (2 mL, 5×10^{-5} M, DMSO) and Zn^{2+} (50 μL, 1×10^{-3} M, H_2O), and then the fluorescence response was checked by adding different amino acids (50 μL, 1×10^{-3} M, H_2O) such as aspartic acid (Asp), cysteine (Cys), alanine (Ala), arginine (Arg), glycine (Gly), histidine (His), leucine (Leu), methionine (Met), proline (Pro), serine (Ser), threonine (Thr), tryptophan (Trp), lysine (Lys) and glutamic acid (Glu) (Fig. 6a). Only after the addition of Cys into the **NPY**·Zn^{2+} complex solution was the fluorescence was quenched completely. Such fluorescence quenching was not observed with other tested amino acids, which clearly shows that the **NPY**·Zn^{2+} complex is selective towards cysteine. To study the sensitivity of the Zn^{2+} complex for the detection of cysteine, the fluorescence of the **NPY**·Zn^{2+} complex was recorded after each incremental addition of cysteine (4 μL, 1×10^{-4} M, H_2O). Upon incremental addition of cysteine, the fluorescence of the zinc complex started decreasing, but does not revert back to the **NPY** fluorescence (Fig. S11†). This quenching of fluorescence may be due to the further complexation of cysteine with the additional coordination sites present at the zinc atom in the **NPY**·Zn^{2+} complex, because cysteine also has more affinity towards metal ions due to the presence of multiple donor atoms like S, O and N atoms. Due to the formation of a stable complex between

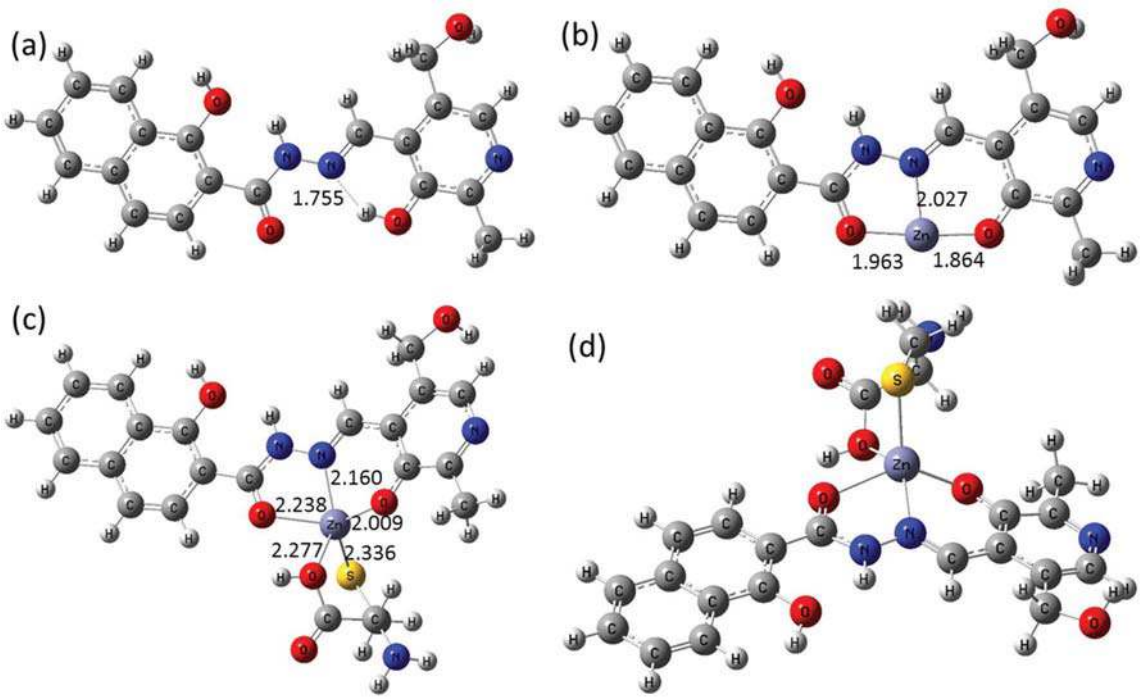

Fig. 5 DFT computed optimized structures of **NPY** (a) and **NPY**·Zn^{2+} (b) and two views of the **NPY**·Zn^{2+}·Cys complex (c and d).

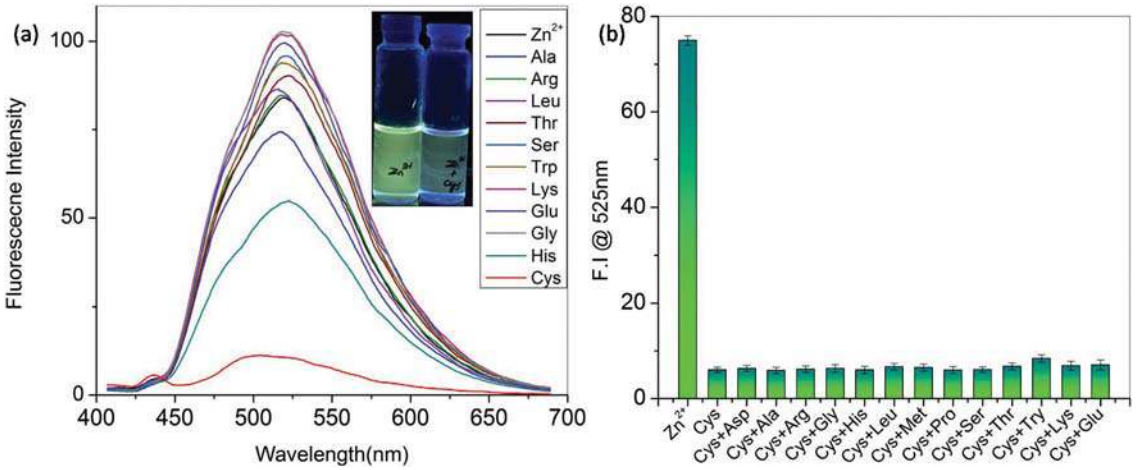

Fig. 6 (a) Fluorescence spectra of the **NPY**·Zn^{2+} complex (2 mL, 5×10^{-5} M, DMSO) upon the addition of Cys and other amino acids (50 μL, 1×10^{-3} M, H_2O). (b) Bar diagram of fluorescence intensity of the **NPY**·Zn^{2+} complex (2 mL, 5×10^{-5} M, DMSO) after adding Cys (50 μL, 1×10^{-3} M, H_2O) and equimolar concentration of the other competitive amino acids (50 μL, 1×10^{-3} M, H_2O).

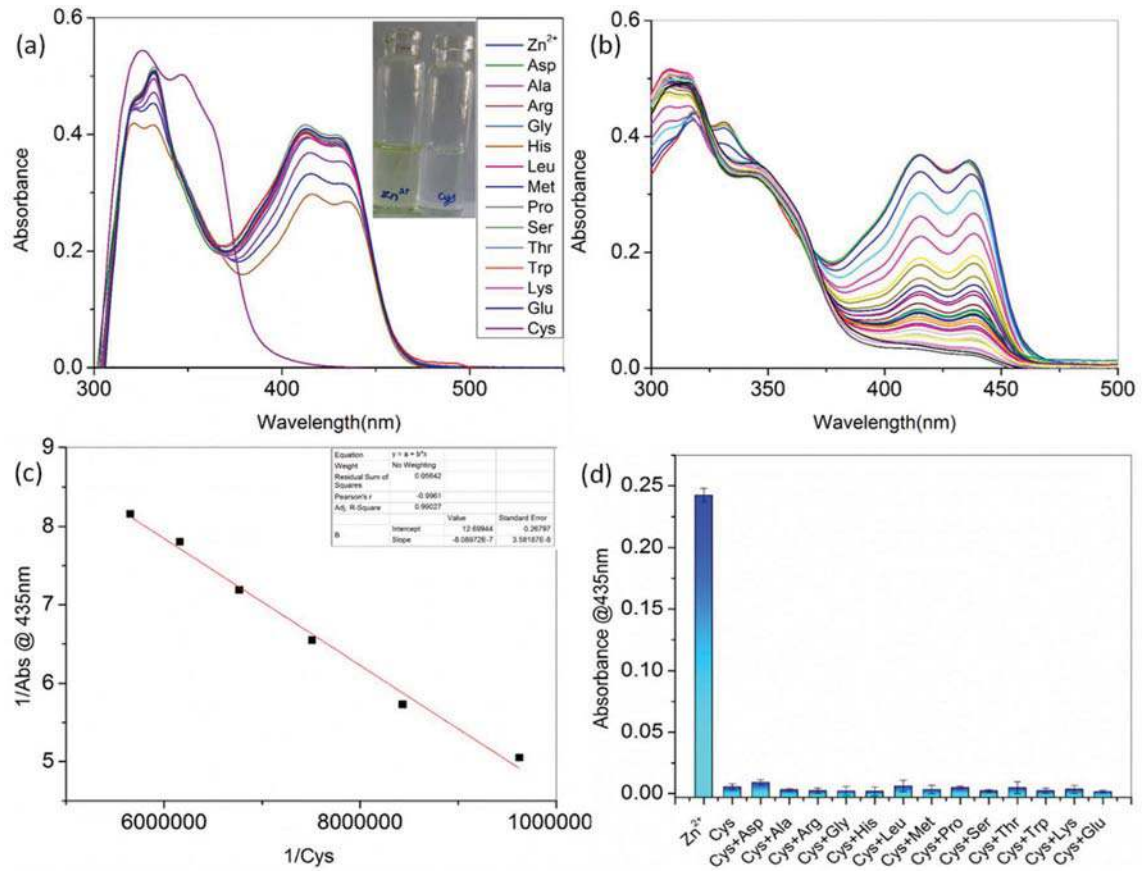

Fig. 7 (a) UV-Visible absorbance spectra of the **NPY**·Zn^{2+} complex (2 mL, 5×10^{-5} M, DMSO) upon the addition of different amino acids (50 μL, 1×10^{-3} M, H_2O) (b) **NPY**·Zn^{2+} complex (2 mL, 5×10^{-5} M, DMSO) upon incremental addition of Cys (5 μL, 1×10^{-5} M, H_2O). (c) B–H plot of the fluorescence curve of the **NPY**·Zn^{2+} complex in the presence of addition of Cys. (d) Bar diagram of absorbance intensity changes of the the **NPY**·Zn^{2+} complex (2 mL, 5×10^{-5} M, DMSO) after adding Cys (50 μL, 1×10^{-3} M, H_2O) and equimolar concentration of the other competitive amino acids (50 μL, 1×10^{-3} M, H_2O).

cysteine and **NPY**·Zn^{2+}, the solution becomes non-fluorescent either due to the electron or charge transfer from the cysteine to the **NPY**·Zn^{2+}. The fluorescence changes of the zinc complex upon addition of cysteine show good selectivity and sensitivity. Using the fluorescence titration data, the association constant of the zinc complex with Cys was found to be 4.02×10^7 M^{-1} and the detection limit down to 6.63×10^{-7} M (Fig. S12a and b†). Further, the interference of the **NPY**·Zn^{2+} complex towards the sensing of cysteine (50 μL, 1×10^{-3} M, H_2O) with various amino acids (50 μL, 1×10^{-3} M, H_2O) was examined (Fig. 6b). No significant changes in the fluorescence profile of the **NPY**·Zn^{2+} complex in the presence of Cys were observed with the addition of the interfering amino acids.

3.6 UV-visible absorption studies of zinc complex with amino acids

To scrutinize the ability of the **NPY**·Zn^{2+} complex as a colorimetric sensor for amino acids, the absorbance changes of the complex solution were analysed with various amino acids. The absorbance response of the **NPY**·Zn^{2+} complex was explored in the presence of different amino acids (50 μL, 1×10^{-3} M, H_2O) such as Asp, Cys, Ala, Arg, Gly, His, Leu, Met, Pro, Ser, Thr, Trp, Lys and Glu. As shown in Fig. 7a, the Zn^{2+} complex shows absorption bands at 330 nm and 435 nm. Interestingly, upon the addition of Cys into the Zn^{2+} complex solution, the absorption peak at 435 nm completely vanished and the formation of a new peak was observed at 348 nm along with the change of colour of the solution instantaneously from light yellow to colourless. However, the addition of other amino acids led to no significant change in the ground state and no colour change of the complex was observed. To further understand the binding nature of the Zn^{2+} complex with cysteine, the concentration dependent absorbance changes were monitored by UV-visible studies. Continuous titration of the Zn^{2+} complex with a subsequent addition of Cys (5 μL, 1×10^{-5} M, H_2O) revealed a continuous intensity decrease in the absorption bands at 435 nm and a new broad band appeared at 348 nm (Fig. 7b). The change in the broad band at 435 nm is because of cysteine, which forms a stable complex with **NPY**·Zn^{2+} through the thiol and amine groups of cysteine. To support that the complex formation occurred between Cys and **NPY**·Zn^{2+}, the complex **NPY**·Zn^{2+}·Cys was isolated in the solid state and characterized. The HRMS analysis showed that the molecular ion peak at m/z = 537.64 was assigned for the $((NPY\text{-}H^+)Zn{\cdot}Cys)^+$ species (Fig. S13†). Also, the recorded UV-Vis absorbance and emission spectra of the synthesized **NPY**·Zn^{2+}·Cys complex were similar to those observed in the solution state (Fig. S7†). Further, the 3D structure of the **NPY**·Zn^{2+}·Cys complex was obtained by DFT calculations and is shown in Fig. 5c and d. Using the UV-Vis titration data, the association constant and the limit of detection of the **NPY**·Zn^{2+} complex for Cys were estimated to be 1.5×10^7 M^{-1} (Fig. 7c) and 2.86×10^{-7} M (Fig. S14†), respectively.

To further check the selectivity of the zinc complex with cysteine, the competitive binding experiments were performed. Zn^{2+} complex was pre-treated with Cys and competitive amino acids (Fig. 7d). No significant variation was observed in the presence of other competing amino acids in comparison with a solution containing only Cys. The zinc complex performed well in the presence of other amino acids and selectively senses cysteine in a competitive environment.

4. Conclusions

In summary, we have introduced a new Schiff base derivative **NPY** of pyridoxal by reacting with 3-hydroxy-2-naphthoic hydrazide. The receptor **NPY** showed a distinct and instantaneous ratiometric fluorescence response in the presence of Zn^{2+} ions due to the coordinative interactions of **NPY** with zinc ions *via* imine-N, pyridoxal-OH and carbonyl-O of naphthyl units. The proposed binding interactions of **NPY** with Zn^{2+} ions were confirmed by ^{1}H-NMR titration experiments, and the probe was utilised for the detection of intracellular Zn^{2+} ions in live HeLa cells. The *in situ* generated **NPY**·Zn^{2+} complex was further used as a sequential sensor to detect the bioactive Cys. With the addition of Cys, the absorbance of the **NPY**·Zn^{2+} complex decreased and also the fluorescence was quenched which allowed two different optical modes for the selective detection of Cys. The detection of Zn^{2+} by **NPY** and the detection of Cys by the **NPY**·Zn^{2+} complex were not affected in the presence of other interfering metal ions and amino acids, respectively.

Conflicts of interest

There are no conflicts of Interest.

Acknowledgements

Dr T. Anand acknowledges the research grant sanctioned (PDF2016/000804) under the DST-SERB National postdoctoral fellowship scheme.

References

1 (*a*) D. T. Quang and J. S. Kim, *Chem. Rev.*, 2010, **110**, 6280–6301; (*b*) A. Bencini and V. Lippolis, *Coord. Chem. Rev.*, 2012, **256**, 149–169; (*c*) Y. Zhou and J. Y. Yoon, *Chem. Soc. Rev.*, 2012, **41**, 52–67.

2 (*a*) R. A. Wapnir, *Protein Nutrition and Mineral Absorption*, CRC Press, 1990; (*b*) M. R. Broadley, P. J. White, J. P. Hammond, I. Zelko and A. Lux, *New Phytol.*, 2007, **173**, 677–696; (*c*) J. J. R. Frausto de Silva and R. J. P. Williams, *The Biological Chemistry of the Elements: The Inorganic Chemistry of Life*, Clarendon Press, Oxford, 1993.

3 (*a*) Q. Huang, Z. Pan, P. Wang, Z. Chen, X. Zhang and H. Xu, *Bioorg. Med. Chem. Lett.*, 2006, **16**, 3030–3033; (*b*) S. Anbu, S. Kamalraj, B. Varghese, J. Muthumary and M. Kandaswamy, *Inorg. Chem.*, 2012, **51**, 5580–5592; (*c*) S. Emami, S. J. Hosseinimehr, S. M. Taghdisi and

S. Akhlaghpoor, *Bioorg. Med. Chem. Lett.*, 2007, **17**, 45–48; (*d*) H. Sakurai, Y. Yoshikawa and H. Yasui, *Chem. Soc. Rev.*, 2008, **37**, 2383–2392.

4 (*a*) J. C. Qin and Z. Y. Yang, *Mater. Sci. Eng., C*, 2015, **57**, 265–271; (*b*) L. J. Tang, M. J. Cai, P. Zhou, J. Zhao, K. L. Zhong, S. H. Hou and Y. J. Bian, *RSC Adv.*, 2013, **3**, 16802–16809.

5 (*a*) C. J. Frederickon, J. Y. Koh and A. I. Bush, *Nat. Rev. Neurosci.*, 2005, **6**, 449–462; (*b*) A. R. Kay, *Trends Neurosci.*, 2006, **29**, 200–206.

6 (*a*) D. W. Choi and J. Y. Koh, *Annu. Rev. Neurosci.*, 1998, **21**, 347–375; (*b*) M. P. Cuajungco and G. J. Lees, *Neurobiol. Dis.*, 1997, **4**, 137–169; (*c*) K. H. Falchuk, *Mol. Cell. Biochem.*, 1988, **188**, 41–48; (*d*) P. J. Fraker and L. E. King, *Annu. Rev. Nutr.*, 2004, **24**, 277–298; (*e*) P. D. Zalewski, I. J. Forbes and W. H. Betts, *Biochem. J.*, 1993, **296**, 403–408; (*f*) C. Jacob, W. Maret and B. L. Vallee, *Proc. Natl. Acad. Sci. U. S. A.*, 1999, **96**, 1910–1914.

7 A. L. Bush, The metallobiology of Alzheimer's disease, *Trends Neurosci.*, 2003, **26**, 207–214.

8 (*a*) A. I. Bush, W. H. Pettingell, G. Multhaup, M. Paradis, J. P. Vonsattel, J. F. Gusella, K. Beyreuther, C. L. Masters and R. E. Tanzi, *Science*, 1994, **265**, 1464–1467; (*b*) M. P. Cuajungco and G. J. Lees, *Neurobiol. Dis.*, 1997, **4**, 137–169.

9 (*a*) A. Voegelin, S. Poster, A. C. Scheinost, M. A. Marcus and R. Kretzschmar, *Environ. Sci. Technol.*, 2005, **39**, 6616–6623; (*b*) E. Callender, *Environ. Sci. Technol.*, 2000, **34**, 232–238.

10 Z. A. Wood, E. Schroder, J. Robin Harris and L. B. Poole, *Trends Biochem. Sci.*, 2003, **28**, 32–40.

11 (*a*) D. M. Townsend, K. D. Tew and H. Tapiero, *Biomed. Pharmacother.*, 2003, **57**, 145–155; (*b*) L. A. Herzenberg, S. C. De Rosa, J. G. Dubs, M. Roederer, M. T. Anderson, S. W. Ela, S. C. Deresinski and L. A. Herzenberg, *Proc. Natl. Acad. Sci. U. S. A.*, 1997, **94**, 1967–1972.

12 (*a*) L. M. Lopez-Sanchez, C. Lopez-Pedrera and A. Rodriguez-Ariza, *Mass Spectrom. Rev.*, 2014, **33**, 7–20; (*b*) M. T. Goodman, K. McDuffie, B. Hernandez, L. R. Wilkens and J. Selhub, *Cancer*, 2000, **89**, 376–382; (*c*) X. Chen, Y. Zhou, X. Peng and J. Yoon, *Chem. Soc. Rev.*, 2010, **39**, 2120–2135.

13 S. Shahrokhian, *Anal. Chem.*, 2001, **73**, 5972–5978.

14 (*a*) I. Ciglenecki, E. Bura-Nakic and G. Inzelt, *Electroanalysis*, 2007, **19**, 1437–1445; (*b*) B. Ge, F. W. Scheller and F. Lisdat, *Biosens. Bioelectron.*, 2003, **18**, 295–302; (*c*) M. Kumar, D. P. S. Rathore and A. K. Singh, *Microchim. Acta*, 2001, **137**, 127–134; (*d*) P. K. Tewari and A. K. Singh, *Analyst*, 2000, **125**, 2350–2355.

15 (*a*) R. H. Yang, W. H. Chan, A. W. M. Lee, P. F. Xia, H. K. Zhang and K. A. Li, *J. Am. Chem. Soc.*, 2003, **125**, 2884–2885; (*b*) M. Royzen, A. Durandin, G. Victor, J. Young, N. E. Geacintov and J. W. Canary, *J. Am. Chem. Soc.*, 2006, **128**, 3854–3855.

16 (*a*) P. Nigam, S. Mohan, S. Kundu and R. Prakash, *Talanta*, 2009, **77**, 1426–1431; (*b*) H. Chen, Y. Wu, Y. Cheng, H. Yang, F. Li, P. Yang and C. Huang, *Inorg. Chem. Commun.*, 2007, **10**, 1413–1415.

17 (*a*) G. Marino, G. Sannia and F. Bossa and B. Verlag, *Biochemistry of Vitamin B_6 and PQQ*. Basel, Switzerland, edn, 1994; (*b*) A. E. Evangelopoulos and A. R. Liss, Chemical and Biological Aspects of Vitamin B_6 Catalysis, New York, 1984.

18 (*a*) M. Strianese, S. Milione, V. Bertolasi and C. Pellecchia, *Inorg. Chem.*, 2013, **52**, 11778–11786; (*b*) E. Oliveira, C. Santos, P. Poeta, J. L. Capelo and C. Lodeiro, *Analyst*, 2013, **138**, 3642–3645; (*c*) D. Sharma, S. K. Sahoo, S. Chaudhary, R. K. Beraand and J. F. Callan, *Analyst*, 2013, **138**, 3646–3650.

19 V. Kumar, A. Kumar, U. Diwan and K. K. Upadhyay, *Dalton Trans.*, 2013, **42**, 13078–13083.

20 A. Hens, A. Maity and K. K. Rajak, *Inorg. Chim. Acta*, 2014, **423**, 408–420.

21 H. A. Benesi and J. H. Hilderbrand, *J. Am. Chem. Soc.*, 1947, **71**, 2703–2707.

22 M. J. Frisch *et al.*, *Gaussian 09 W, Revision A.1*, Gaussian Incorp, Wallingford, CT, 2009.

